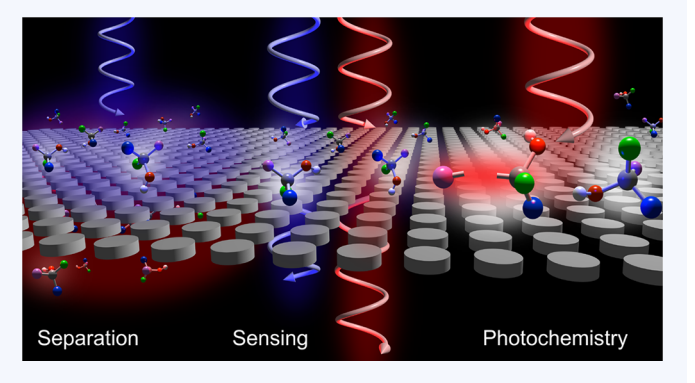


Nanophotonic Platforms for Chiral Sensing and Separation

Michelle L. Solomon, †, London, Amr A. E. Saleh, †, Lisa V. Poulikakos, London, John M. Abendroth, Loza F. Tadesse, and Jennifer A. Dionne *,†,||6

CONSPECTUS: Chirality in Nature can be found across all length scales, from the subatomic to the galactic. At the molecular scale, the spatial dissymmetry in the atomic arrangements of pairs of mirror-image molecules, known as enantiomers, gives rise to fascinating and often critical differences in chemical and physical properties. With increasing hierarchical complexity, protein function, cell communication, and organism health rely on enantioselective interactions between molecules with selective handedness. For example, neurodegenerative and neuropsychiatric disorders including Alzheimer's and Parkinson's diseases have been linked to distortion of chiral-molecular structure. Moreover, Damino acids have become increasingly recognized as potential



biomarkers, necessitating comprehensive analytical methods for diagnosis that are capable of distinguishing L- from D-forms and quantifying trace concentrations of D-amino acids. Correspondingly, many pharmaceuticals and agrochemicals consist of chiral molecules that target particular enantioselective pathways. Yet, despite the importance of molecular chirality, it remains challenging to sense and to separate chiral compounds. Chiral-optical spectroscopies are designed to analyze the purity of chiral samples, but they are often insensitive to the trace enantiomeric excess that might be present in a patient sample, such as blood, urine, or sputum, or pharmaceutical product. Similarly, existing separation schemes to enable enantiopure solutions of chiral products are inefficient or costly. Consequently, most pharmaceuticals or agrochemicals are sold as racemic mixtures, with reduced efficacy and potential deleterious impacts.

Recent advances in nanophotonics lay the foundation toward highly sensitive and efficient chiral detection and separation methods. In this Account, we highlight our group's effort to leverage nanoscale chiral light-matter interactions to detect, characterize, and separate enantiomers, potentially down to the single molecule level. Notably, certain resonant nanostructures can significantly enhance circular dichroism for improved chiral sensing and spectroscopy as well as high-yield enantioselective photochemistry. We first describe how achiral metallic and dielectric nanostructures can be utilized to increase the local optical chirality density by engineering the coupling between electric and magnetic optical resonances. While plasmonic nanoparticles locally enhance the optical chirality density, high-index dielectric nanoparticles can enable large-volume and uniform-sign enhancements in the optical chirality density. By overlapping these electric and magnetic resonances, local chiral fields can be enhanced by several orders of magnitude. We show how these design rules can enable high-yield enantioselective photochemistry and project a 2000-fold improvement in the yield of a photoionization reaction. Next, we discuss how optical forces can enable selective manipulation and separation of enantiomers. We describe the design of low-power enantioselective optical tweezers with the ability to trap sub-10 nm dielectric particles. We also characterize their chiral-optical forces with high spatial and force resolution using combined optical and atomic force microscopy. These optical tweezers exhibit an enantioselective optical force contrast exceeding 10 pN, enabling selective attraction or repulsion of enantiomers based on the illumination polarization. Finally, we discuss future challenges and opportunities spanning fundamental research to technology translation. Disease detection in the clinic as well as pharmaceutical and agrochemical industrial applications requiring largescale, high-throughput production will gain particular benefit from the simplicity and relative low cost that nanophotonic platforms promise.

INTRODUCTION

Observed from subatomic particles to the macroscale, chiral structure dictates function. Chiral properties are particularly notable in molecules including amino acids, proteins, sugars,

Received: August 31, 2019 Published: January 8, 2020

[†]Department of Materials Science and Engineering, Stanford University, Stanford, California 94305, United States

[‡]Department of Engineering Mathematics and Physics, Faculty of Engineering, Cairo University, Giza 12613, Egypt

Department of Bioengineering, Stanford University, Stanford, California 94305, United States

Department of Radiology, Stanford University, Stanford, California 94305, United States

enzymes, and a variety of pharmaceuticals and agrochemicals. In a molecular ensemble, enantiomers are most often distinguished using chiral-optical spectroscopies that analyze either circular dichroism or circular birefringence. These spectral signatures result from the preferential absorption and differential phase delay, respectively, of left- or right-handed circularly polarized light.

Historically, the first observation of chiral-optical activity dates to 1811 when Arago observed colors in sunlight after passing through quartz - which has a chiral crystal structure of achiral SiO₂ atomic subunits - placed between two polarizers.¹ Biot later attributed the phenomenon to optical rotation in the plane of polarization at different wavelengths (optical rotatory dispersion).² The discovery of left- and right-handed circular polarization states of light by Fresnel in 1824 led to the conclusion that this rotation of linearly polarized light (composed equally of left- and right-handed circular polarization) resulted from different refractive indices for opposite circular polarization states of light in the chiral medium. Pasteur's discovery of molecular handedness via observation of the optical rotation of tartaric acid in 1848 extended the scope of these phenomena from the dissymmetric arrangement of crystalline building blocks to the helicoidal arrangement of atoms in molecules themselves. 1,3,4

Significant advances in optical instrumentation in the 1960s, particularly the advancement of piezo-optical birefringence modulators, furthered research efforts in molecular optical activity and enabled these spectroscopies to find widespread use as analytical tools in biochemistry. 5,6 For example, the insights on secondary and tertiary molecular structure provided by these spectroscopic techniques enabled important progress in the development of biochemicals, e.g., for agrochemical and pharmaceutical applications, where chirality plays a central role. However, chiral-optical spectroscopies are inherently limited in sensitivity due to the scale-mismatch between the helical pitch of atoms in molecules and the wavelength of ultraviolet, visible, and near-infrared light. 8,9 Thus, highthroughput industrial applications and bioanalytical techniques that require detection of trace amounts of chiral molecules are prohibitively challenged by the small magnitude of circular dichroism.

Recent advancements in the field of nanophotonics offer solutions to overcome these challenges by enhancing chiral light-matter interactions. For example, nanostructured optical antennas scale light below the diffraction limit to approach molecular dimensions at optical frequencies. Simultaneously, these nano-optical antennas preserve or convert the circular polarization of incident light to allow for enhancement in the local chiral field. This local optical chirality density was derived by Lipkin in 1964. 10 Subsequently, metallic nanostructures with chiral geometries, including individual nanoparticles, nanoparticle assemblies, and DNA origami, were used to generate high optical chirality density and enhanced circular dichroism with orders-of-magnitude larger amplitudes than typically observed for chiral molecules. 7,11-42 In 2010, Tang and Cohen showed how such enantioselective enhancements could amplify selectively the rate of excitation of chiral molecules. 8,43 However, these chiral-optical enhancements are generally still insufficient for practical, high-efficiency, and highsensitivity chiral sensing, separation, and asymmetric synthesis, particularly when compared to chiral column chromatography, 44 requiring new strategies to enhance enantioselective interactions.

In this Account, we highlight emerging strategies to enhance optical chirality density based on rational design of metallic and dielectric nanostructures. These structures systematically manipulate electric and magnetic light—matter interactions, including the amplitude and phase of the local field, enabling precise interaction with chiral molecules to tailor their absorptivity, emission, and vibrational amplitudes. We then discuss the application of these nanophotonic platforms to (1) distinguish chiral molecules for high-sensitivity biochemical sensing; (2) amplify enantiomeric excesses in asymmetric chemical reactions; and (3) enable all-optical strategies for enantiomer separations.

OPTICAL CHIRALITY ENHANCEMENT WITH DIELECTRIC NANOSTRUCTURES FOR CHIRAL SENSING

Circular dichroism (CD) spectroscopy is used to characterize optically active species, ranging from small-molecule analytes possessing a single asymmetric chiral center to hierarchically more complex molecular assemblies.⁴⁵ The difference in absorption of circularly polarized light (CPL) by chiral molecules provides a method to distinguish isomers and determine enantiomeric excess of mixed analytes, necessary for characterizing products in asymmetric synthesis. 46-48 Moreover, spectral signatures that are indicative of common structural motifs enable monitoring secondary and tertiary conformations of biomolecules including peptides, proteins, and oligonucleotides. Spectral changes in CD can therefore be used for diverse bioanalytical applications such as understanding protein aggregation associated with disease onset and progression, 49,50 characterizing conformational changes of aptamers induced by target binding, 51,52 and testing environmental stability of oligonucleotides.

Typically, differential absorption of CPL by chiral molecules lies orders of magnitude below the corresponding total absorption amplitude of unpolarized light due to dimensional mismatch of the arrangement of molecular bonds and the pitch of CPL. Measuring relative excess of a chiral target over its mirror image requires high sample concentrations, long optical path lengths, and signal amplification. These drawbacks limit sensitivity, and thus utility, of CD spectroscopy as an analytical technique.

To overcome these challenges, subwavelength nanophotonic structures that enhance both the intensity and chirality of evanescent fields can be used to selectively amplify the rate of light absorption by enantiomers over their mirror image isomers. Upon illumination with CPL, evanescent fields surrounding a nanostructure can take on arbitrary polarization states, with the potential to enhance the optical chirality density, C. Compared to CPL in vacuum alone $(C_{\text{CPL}} = \pm \frac{\epsilon_0 \omega}{2c} E_0^2)$, C near a nanostructure takes the form:

$$C^{\pm} = -\frac{\omega}{2c^2} \operatorname{Im}(\mathbf{E}^* \cdot \mathbf{H}) = -\frac{\omega}{2c^2} |\mathbf{E}||\mathbf{H}| \cos(\beta_{i\mathbf{E},\mathbf{H}})$$
(1)

where ϵ_0 is the permittivity of free space, ω is the angular frequency, c is the speed of light, E_0 is the incident electric field magnitude, and E and H represent the complex electric and magnetic field vectors, respectively. The value, $\beta_{iE,H}$, describes the phase angle between iE and H.

Optical chirality is proportional to the rate of absorption by a chiral molecule, as given by

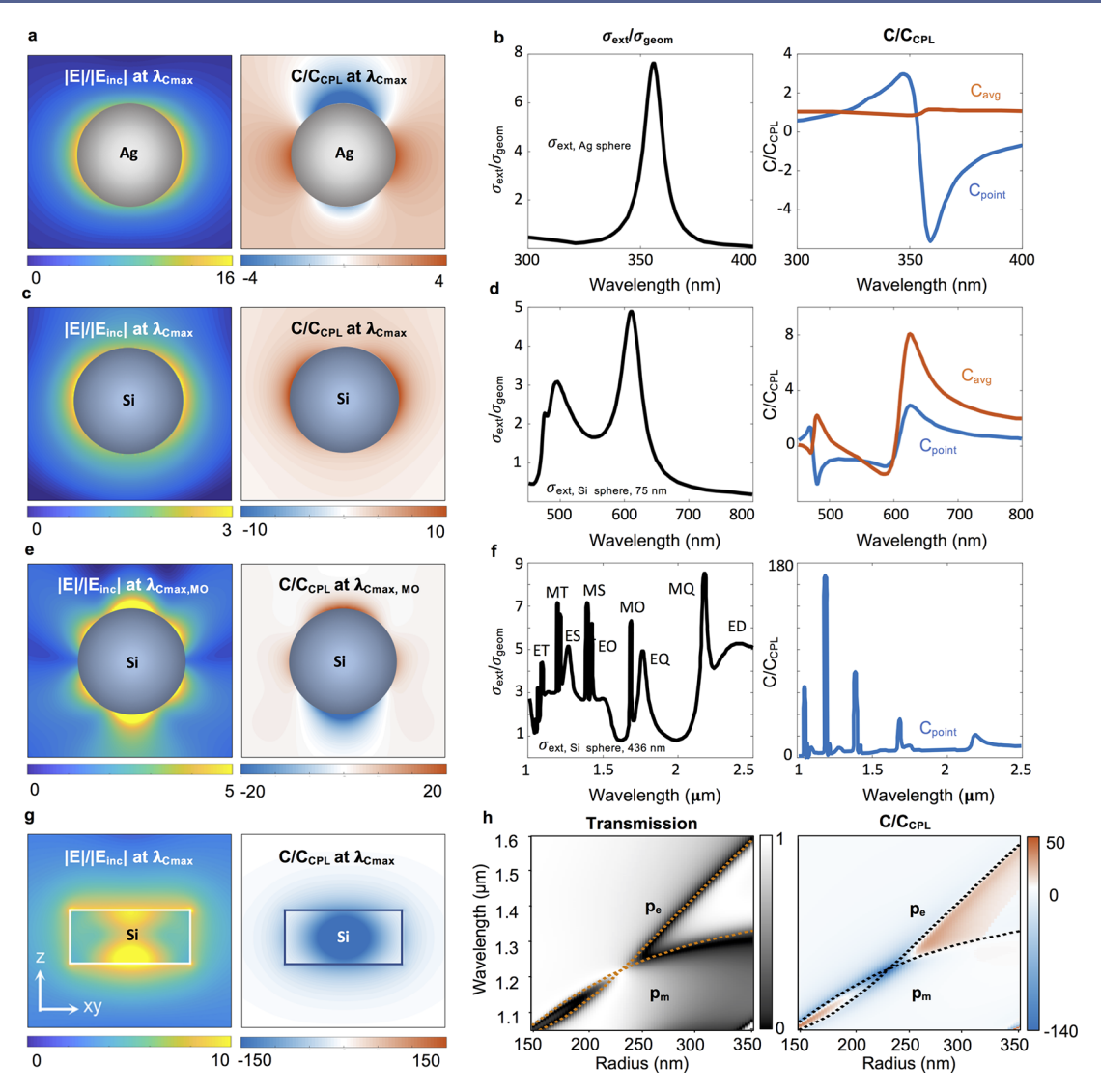


Figure 1. (a) Enhancements in electric field amplitude (left) and optical chirality (right) with 10 nm radius silver sphere at 359 nm. (b) Scattering spectrum (left) of plasmonic particle, plotted with optical chirality enhancement (right) at a point 1 nm above the sphere, and averaged in 1 nm thick shell around the surface. (c) Enhancements in electric field amplitude (left) and optical chirality (right) with 75 nm radius silicon sphere at 625 nm. d) Scattering spectrum (left) of 75 nm Si sphere plotted against optical chirality enhancement (right) at a point 1 nm above the sphere, and averaged in a 1 nm-thick shell around the surface (right). (a-d) Adapted with permission from ref 54. Copyright 2013 American Physical Society. (e) Field maps of Si nanosphere supporting higher-order moments that improve electric field amplitude (left) and optical chirality enhancement (right), plotted at 1684 nm. (f) Scattering spectrum of 436 nm sphere (left), with maximum point enhancement in C (right). (e, f) Adapted with permission from ref 56. Copyright 2017 American Chemical Society. (g) Uniform-sign, large-area enhancements in C are achieved with arrays of Si disks. Electric field amplitude enhancement (left) and C/C_{CPL} (right) of square array of Si disks with r = 230 nm, h = 200 nm, and lattice parameter a = 1000 nm at 1219 nm. (h) Transmission spectra with disk radius 150–350 nm (left), compared with enhancements in C (right). (g, h) Adapted from ref 57. Copyright 2019 American Chemical Society.

$$A^{\pm} = \frac{\omega}{2} (\alpha'' |\mathbf{E}|^2 + \mu_0^2 \chi'' |\mathbf{H}|^2) \mp \frac{2}{\epsilon_0} G'' C$$
 (2)

where α'' , χ'' , and G'' are the imaginary components of the electric, magnetic, and chiral polarizability of the molecule, respectively, and μ_0 is the free-space magnetic permeability. As the CD of a molecule is given by the differential absorption of right- and left-CPL (CD $\propto A^+ - A^-$), by the above equations, CD $\propto 4/\epsilon_0 G'' C$, illustrating that enhancing optical chirality through manipulation of near fields is one factor that can lead to higher sensitivity CD, in addition to other far-field effects such as interference. 8,54,55

The use of chiral plasmonic nanostructures to engineer enhancements in C has received considerable attention.³⁰ In

plasmonic structures, C enhancement arises largely from electric multipolar resonances. For example, achiral plasmonic spheres generate local enhancements in C (Figure 1a,b) near the dipolar plasmon resonance. However, enhancements are spatially varying in sign (handedness)⁵⁴ and are therefore negligible when averaged over the particle surface (Figure 1b).

While plasmonic responses are dominated by electric resonances upon irradiation, high-refractive-index dielectric nanoparticles support both electric and magnetic multipolar Mie resonances (Figure 1c,d). For the example of a 75 nm radius Si sphere, two resonances are present between 500 and 700 nm (Figure 1d, left panel), a lowest order magnetic dipole and a second-lowest order electric dipole. The presence of magnetic resonances enables further control of the chiral-optical proper-

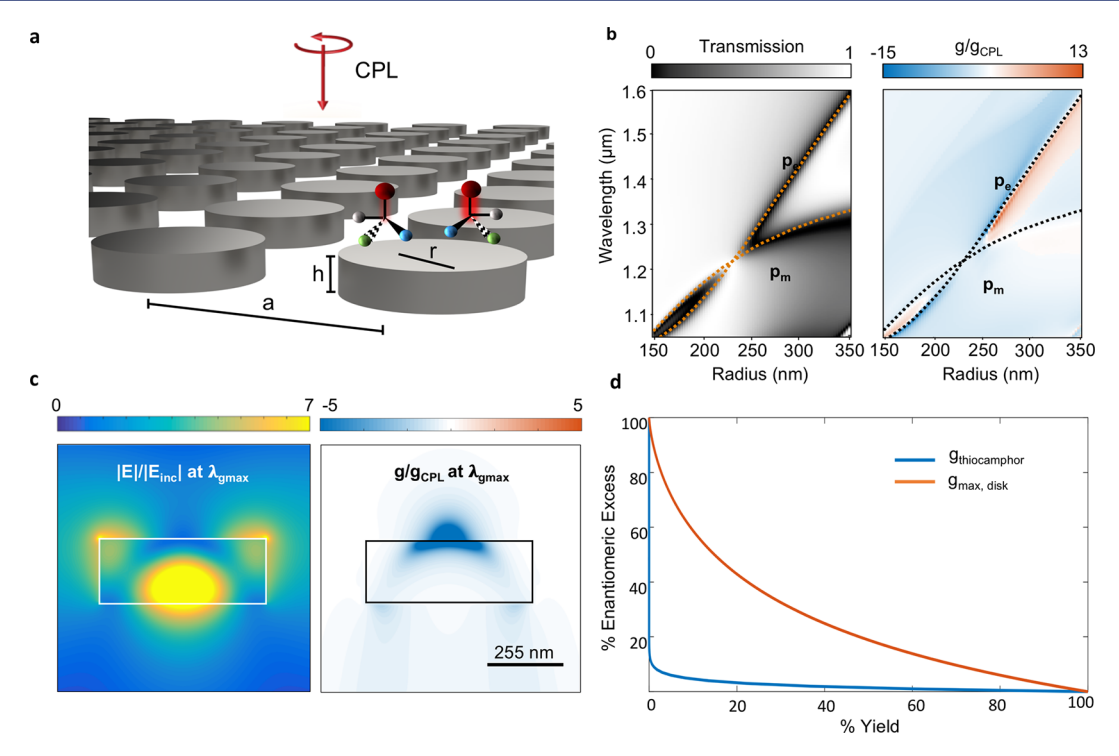


Figure 2. (a) Silicon nanoparticles can asymmetrically enhance absorption of right- versus left-handed CPL in chiral molecules, leading to photolysis. (b) Transmission spectra with disk radius 150–350 nm (left), compared with enhancement in g (right), which reaches a maximum of 15-fold. (c) Electric field amplitude enhancement when g/g_{CPL} is maximized (left) in a square array of Si disks (r = 255 nm, h = 200 nm, a = 1000 nm). Map of g/g_{CPL} (right) shows large, uniform-sign enhancements. (d) Photoionization of thiocamphor predicted based first-order kinetic model. (e) Increases in dissymmetry factor from disk array give 20% enantiomeric excess with 52% yield, up from <1% yield. Adapted from ref 57. Copyright 2019 American Chemical Society.

ties. As a result, it is possible to attain *single-sign* enhancements of C (Figure 1c).

This effect can be further increased via multipolar modes of high-index dielectric nanospheres of different radii (Figure 1e). For example, silicon spheres of radius 436 nm exhibit several resonances for wavelengths between 2.5 and 3.5 μ m, corresponding to magnetic and electric multipolar modes ranging from second (dipolar) to thirty-second order. Importantly, the maximum enhancements in C (eq 1) occur near the magnetic multipolar resonances, indicating that a strong magnetic field is a significant design rule.

It is also notable that, as mode order increases, so too does quality factor (as evidenced by sharper line widths in Figure 1f, left) and C/C_{CPL} . In particular, we see improvements in C of 33fold, 78-fold, and 169-fold (at the magnetic 8-polar, 16-polar, and 32-polar modes respectively) as the full-width halfmaximum of the mode ranges from 20 nm down to 3 nm and finally 2 nm (Figure 1f, left). These stronger enhancements occur due to the lengthened lifetimes of the higher-order resonances, building electromagnetic field strength within the particle (Figure 1e, left). However, these higher-order resonances are also characterized by the many-lobed distribution in Figure 1e. Thus, $C/C_{\rm CPL}$ is again both positive and negative in sign around the sphere as the phase of the standing wave varies from lobe to lobe. Accordingly, while higher-order modes attain larger field strength and higher local enhancements, they suffer from losses in global enhancement.

In order to achieve enhancements that are both large and spatially consistent, we introduced high-index-dielectric nanodisk arrays. ⁵⁷ The crucial advantage of nanodisks over spheres lies in the independent tunability of the electric and magnetic

resonances via disk aspect ratio (Figure 1g). While the electric multipolar resonances depend primarily on disk radius, the magnetic multipolar resonances are controlled predominantly by the height. Therefore, when the radius increases while the height is fixed, the electric mode red-shifts more significantly than the magnetic. Thus, independent optimization of the phase between the resonances and the strength of the optical response is possible.

As the modes shift unequally, the two resonances cross (Figure 1h), marking a Kerker-like condition where the transmission approaches unity. 58,59 Here, as both resonances occur at the same frequency and with similar line widths, the phase of the electric and magnetic field shifts identically. Consequently, not only are the electric and magnetic fields strong, but also they maintain circular polarization, maximizing the enhancement in C. Specifically, here we attain a maximum 138-fold enhancement outside the disk relying only on lowquality-factor dipolar modes, which previously exhibited enhancements less than 20-fold. Furthermore, like the dipolar modes studied in García-Etxarri et al.,54 the studied nanodisk modes show more spatial uniformity than the higher-order modes studied in Ho et al. 56 Therefore, the enhancement in optical chirality is consistent in sign around the entire surface, leading to a significant volumetric enhancement in addition to the high local enhancements. The additional degrees of freedom in the nanodisk have allowed us to not only optimize the electric and magnetic fields, but also the phase between them. Accordingly, this disk array enables volumetric enhancement of optical chirality using dipolar modes alone. This effect can be seen in other geometries as well, including holey disks. 60 Such independent spectral tunability of electric and magnetic

multipolar modes makes these metasurfaces powerful tools to achieve high chiral-optical volumetric enhancement in spatial regions easily accessible by chiral analytes.

HARNESSING AMPLIFIED ELECTROMAGNETIC CHIRALITY DENSITY FOR ENANTIOSELECTIVE PHOTOCHEMISTRY

Chemical methods to separate enantiomers include chiral chromatography, autocatalysis, self-replication, and chiralselective amplification; these methods are the current industry norm but are analyte-specific and lack atom-efficiency. Optical approaches based on resonant chiral light-molecular interactions have the potential to streamline enantiomer separation and enantioselective photochemistry, providing a more generalizable platform for a multitude of analytes and improving atomefficiency. For example, circularly polarized illumination can influence enantioselective conversion in photochemical reactions, even from racemic mixtures. As a result of CD, enrichment in the concentration of a single enantiomer over its mirror image has been attained by preferential photoionization or photodestruction of a wide range of compounds, 61 including camphor⁶² and various amino acids.⁶³ Alternatively, interconversion between metastable states in photoisomerization of molecular switches and rotors such as azobenzene derivatives⁶⁴ and sterically overcrowded alkenes⁶⁵ provide strategies for reversible formation of one enantiomer over another with light. While enantioselectivity in photochemical reactions via asymmetric photolysis of chiral molecules was demonstrated as early as 1929, 66,67 preferred photodestruction has historically suffered from low enantiomeric excess and yield. 62

The figure of merit for such an all-optical approach, Kuhn's dissymmetry factor, g_i^{68} is defined as preferential absorption of light of one handedness normalized by total absorption, ⁴³

$$g = \frac{2(A^{+} - A^{-})}{A^{+} + A^{-}} \tag{3}$$

Similar to CD, Kuhn's dissymmetry factor is proportional to the optical chirality density, C, as seen when A^{\pm} is substituted with the definition in eq 2.

$$g = -\left(\frac{G''}{\alpha''}\right)\left(\frac{8C}{\omega\epsilon_0 |\mathbf{E}|^2}\right) \tag{4}$$

Thus, the dissymmetry factor is proportional to C, but inversely proportional to electric field amplitude. To study the effect that nanophotonic structures have on dissymmetry, and therefore asymmetric photolysis, we define enhancement in dissymmetry as $g/g_{\rm CPL}$. In the studied small-molecule regime, the dissymmetry factor under CPL irradiation alone, or $g_{\rm CPL}$ has previously been defined as $g_{\rm CPL} = -4G''/c\alpha$, ⁵⁶ where c is the speed of light. Thus, enhancements can be defined solely in terms of the electromagnetic field surrounding a nanophotonic structure. ⁵⁶

$$\frac{g}{g_{CPL}} = \frac{2c}{\omega \epsilon_0} \frac{C}{|\mathbf{E}|^2} = -\frac{1}{\omega c} \frac{|\mathbf{E}||\mathbf{H}|\cos(\beta_{i\mathbf{E},\mathbf{H}})}{|\mathbf{E}|^2}$$
(5)

In our research, we have found significant potential for high-index dielectric nanostructures to catalyze such light-mediated reactions. S4,S6,S7 Here, we focus on the enhancements in dissymmetry that are possible using a nanodisk metasurface (Figure 2a). Like the enhancements in optical chirality seen above, the optimal condition for enhancement in dissymmetry

occurs near the overlap of the electric and magnetic dipole modes (Figure 2b). In contrast to C enhancements, which occur on-resonance (Figure 1), the maximum enhancements in g (eq 5) are found slightly off-resonance. At this wavelength, a strong magnetic field outside the disk and a relatively weak electric field lead to a single-sign enhancement in g in a region readily accessible by an analyte (Figure 2c). The observed maximum in $g/g_{\rm CPL}$ is 15-fold at 1297 nm, more than 5-fold that attainable at the dipole mode of silicon nanospheres. Optimal enhancements in g occur in proximity to, but not directly on, the Kerker-like condition, marking slight electric and magnetic detuning as a crucial design rule for Kuhn's dissymmetry factor.

To study the potential of such a metasurface to separate a racemic chemical mixture, we consider first-order photo-decomposition kinetics of thiocamphor, as camphor derivatives can undergo a ring-opening photoionization reaction. We design a metasurface to maximize g/g_{CPL} at 520 nm, where $g_{thiocamphor}$ peaks at 0.04. We model the relationship between enantiomeric excess (y) and yield(x) as 62

$$x = \frac{1}{2} \left[\left(\frac{1+y}{1-y} \right)^{1/2 - 1/g} + \left(\frac{1+y}{1-y} \right)^{-1/2 - 1/g} \right]$$
 (6)

Figure 2d illustrates enantiomeric excess versus yield using this model, including the result that CPL alone could attain a 20% enantiomeric excess in thiocamphor, but with a mere 0.004% yield. Thus, accomplishing measurable enantiomeric excess requires the destruction of a majority of molecules in the studied mixture, regardless of their handedness. However, in the presence of the nanodisk metasurface and the 15-fold enhancement in dissymmetry, it is projected that a 20% enantiomeric excess with up to a 52% yield is possible, a significant step toward pharmaceutically relevant reactions. However, to move toward >90% enantiomeric excess with >80% yield for practical and viable alternatives to asymmetric synthesis and chiral separation, additional optimization is necessary. Notably, magnetic field strength must be improved via metasurface design, and material limitations must be overcome as relevant molecules are typically resonant in the ultraviolet regime, where it is unusual for dielectric materials to have high refractive index with low losses. We anticipate that progress can be made through innovative tuning of high-quality-factor dipolar resonances of lower-index UV-lossless optical lattices. 69 Finally, these nanophotonic platforms may enable asymmetric amplification of small enantioselective differences in absorption of chiral light with kinetic control by taking advantage of self-catalyzed crystallization and surface interactions under appropriate environmental conditions simultaneously, analogous to recent reports of enantiomer separations using ferromagnetic materials. 70,77

ENANTIOSELECTIVE PLASMONIC TWEEZERS

Sculpted electromagnetic beams can serve as optical tweezers, allowing small objects to be accelerated, manipulated, or trapped with light alone. These beams can exhibit remarkable enantioselectivity of optical forces, making light-based techniques appealing and more efficient alternatives to chemical methods for enantiomer manipulation and separation. For chiral particles, optical forces are determined by the electric and magnetic field gradients as well as spin and orbital angular momentum, and thus can become selective to the particle handedness. For nanoscale chiral particles, the total optical forces on enantiomers can be written as the service of the particle forces on enantiomers can be written as the service of the particle forces on enantiomers can be written as the service of the particle forces on enantiomers can be written as the service of the particle forces on enantiomers can be written as the service of the particle forces on enantiomers can be written as the service of the particle forces on enantiomers can be written as the service of the particle forces of the service of the particle forces of the service of the service of the service of the particle forces of the service of the serv

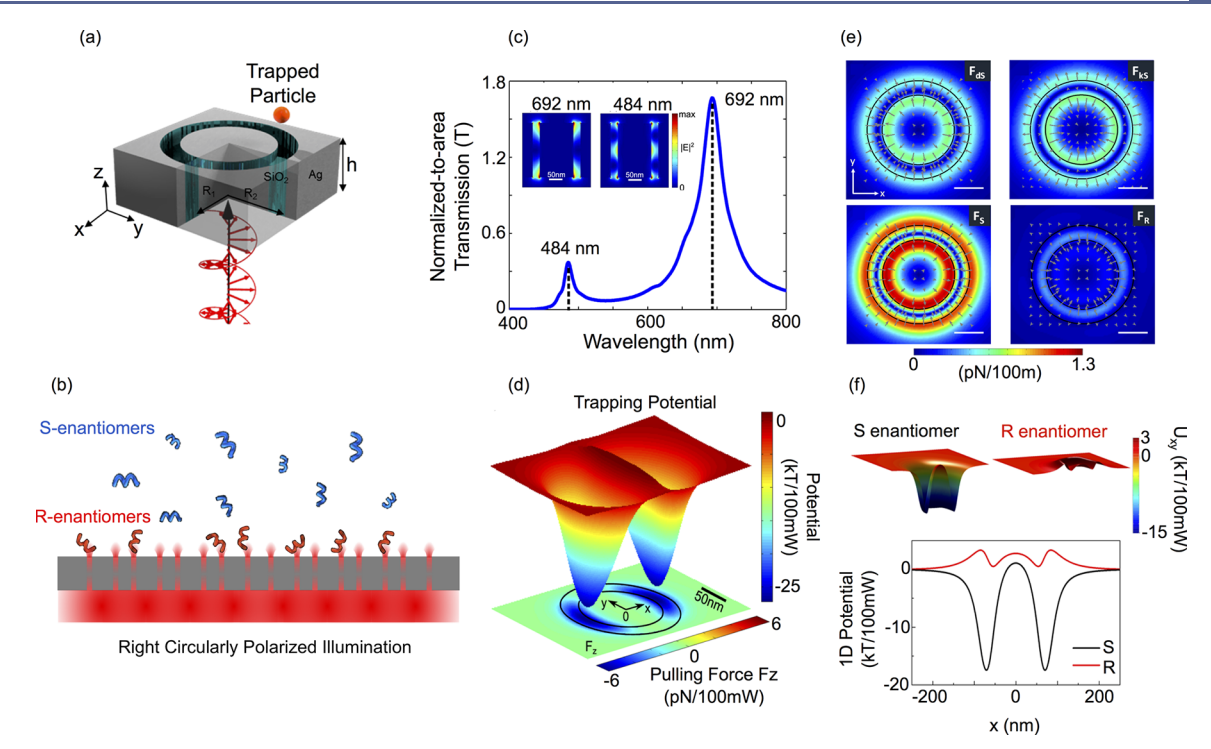


Figure 3. (a) Schematic of coaxial plasmonic tweezers. Adapted from ref 81. Copyright 2016 American Chemical Society. (b) Use of coaxial plasmonic tweezer array for selective trapping of chiral objects. (c) Transmission spectrum of 150 nm thick silver coaxial aperture with 120 nm core diameter and 25 nm silica channel with electric field intensity distribution at the two resonance peaks (inset). Adapted from ref 83. Copyright 2012 American Chemical Society. (d) Transverse trapping potential well (U_{xy}) and pulling force (F_z) on a 10 nm dielectric particle located 20 nm from the aperture, linear polarization. (e) Transverse optical forces calculated 20 nm away from the aperture under L-CPL. F_{ds} and F_{ks} denote dielectric gradient force and chiral gradient force on an S-enantiomer, respectively. F_S and F_R denote total optical forces on an S- and S-enantiomer with S = S

$$\mathbf{F} = \frac{\operatorname{Re}(\alpha_{ee})}{4} \nabla |\mathbf{E}|^2 + \operatorname{Im}(\alpha_{ee}) \left(\frac{\omega}{2\varepsilon_0} \nabla \times \mathbf{L}_{s} \right) + \operatorname{Im}(\alpha_{em}) \frac{1}{2} \nabla \operatorname{Im}(\mathbf{E} \cdot \mathbf{H}^*) - \operatorname{Re}(\alpha_{em}) \nabla \times \mathbf{S}$$
(7)

where $\alpha_{\rm ee}$ is the electric polarizability and $\alpha_{\rm em}$ is the electromagnetic polarizability and is directly related to the chirality of particle (κ) as 82

$$\alpha_{\rm em} = -12\pi r^3 \frac{j\kappa \sqrt{\varepsilon_0 \mu_0}}{(\varepsilon_r + 2\varepsilon_{\rm rm})(\mu_r + 2) - \kappa^2}$$
 (8)

Here, $\varepsilon_{\rm r}$ and $\mu_{\rm r}$ are the relative permittivity and permeability of the particle, $\varepsilon_{\rm rm}$ is the relative permittivity of the surrounding medium, and r is the particle radius. Notably, the sign of the electromagnetic polarizability, $\alpha_{\rm em}$, is determined by that of κ which describes the particle handedness. For achiral particles, the chirality, κ , and consequently the polarizability, $\alpha_{\rm em}$, both reduce to zero.

From eq 7, we note that the total optical forces on enantiomers are directly proportional to two main components: the electric field intensity gradient $(\nabla |\mathbf{E}|^2)$ and the optical chirality density gradient $(\nabla |\mathbf{H}(\mathbf{E}\cdot\mathbf{H}^*))$. Interestingly, the contribution of the second component for a given electromagnetic field is directly determined by the sign of the polarizability, $\alpha_{\rm em}$, and the particle chirality, κ . Thus, selective trapping of enantiomers can be attained by boosting the contribution of $(\nabla |\mathbf{Im}(\mathbf{E}\cdot\mathbf{H}^*))$ to enhance the contrast between the total optical forces of each handedness.

Our lab has introduced coaxial plasmonic tweezers to enable direct trapping and manipulation of dielectric particles as small as 2 nm. ⁸³ As illustrated in Figure 3a, these tweezers consist of a nanoscale dielectric channel, a metallic core and a metallic cladding. Illumination of this coaxial fiber excites surface plasmons at each metal-dielectric interface that propagate along the fiber resulting in highly localized electromagnetic fields and field gradients that direct the particle toward the fiber. The optical power requirements of these tweezers are considerably lower than conventional optical tweezers as was experimentally verified by Yoo et al. ⁸⁴

In addition to the strong field gradients, the circular symmetry of the coaxial apertures is instrumental in enhancing the contrast in the total optical forces on chiral particles under CPL. In particular, this symmetry aligns the maxima of the force components from the electric field gradient and the chirality density gradient over the aperture, enabling the local addition or subtraction of these different force components and facilitating enantioselective optical trapping (Figure 3b). When an array of coaxial tweezers is illuminated with right-handed CPL, only particles with matching chirality will be trapped, while particles with opposite handedness will be pushed away from the coaxial aperture.

Figure 3c depicts the transmission spectrum of a 150 nm-tall coaxial aperture calculated using finite-difference time-domain (FDTD) methods. The spectrum shows two peaks at 692 and 484 nm corresponding to the two Fabry—Perot resonances of the aperture (Figure 3c, inset). When a nanoscale dielectric particle interacts with the near-field, the particle experiences a strong, trapping potential well which is deep enough (>10 kT)

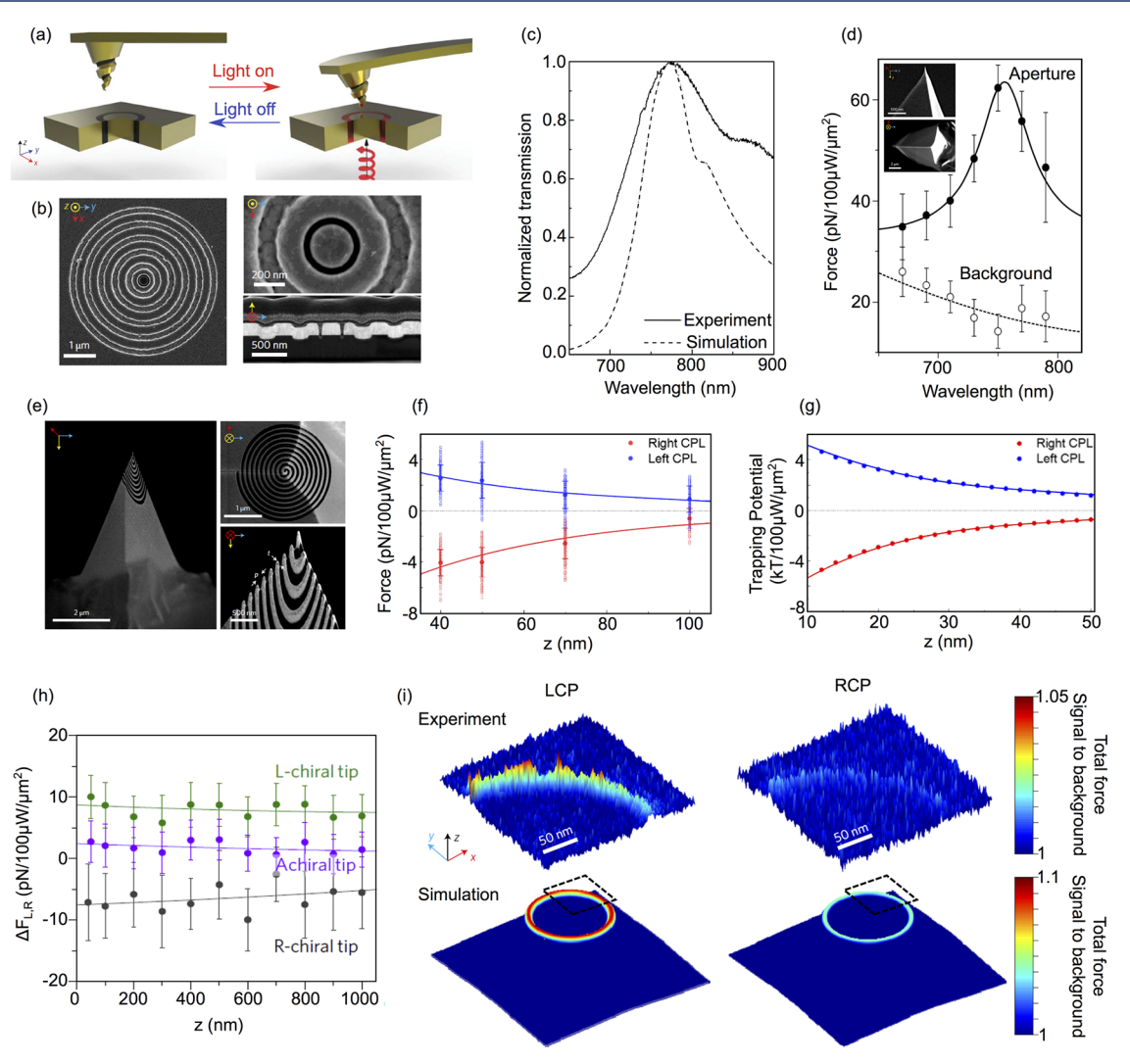


Figure 4. (a) Schematic of CFM technique to measure chiral optical forces at the nanoscale. (b) Scanning electron microscopy (SEM) image of the coaxial plasmonic tweezers under study. (c) Normalized transmission spectrum of coaxial aperture measured experimentally and spectrum calculated using FDTD. (d) Optical force spectra measured right on top of the aperture and away from the aperture. Inset: silicon AFM tip used to measure these forces. (e) SEM image of a gold-coated chiral tip. (f) Transverse optical forces measured using the left-handed tip under right- and left-CPL and (g) calculated trapping potential. (h) Difference in total forces with right- and left-CPL illumination for both left- and right-handed tips and an achiral tip. (i) Chiral optical force map measured over one quadrant of coaxial aperture under both left- and right-CPL illumination and corresponding simulations. Adapted from ref 85. Copyright 2017 Springer Nature.

to stably confine the particle (Figure 3d). However, with linearly polarized illumination, this potential provides no selectivity for enantiomers.⁸¹

When illuminated with CPL, both the dielectric chiral gradient force distributions overlap over the coaxial aperture (Figure 3e). Consequently, the contrast in the total optical forces between the different enantiomers can be maximized (Figure 3e, bottom). The total optical force on the S-enantiomer reaches 1.23 pN/100 mW, while it is only 0.35 pN/100 mW for the R-enantiomer. Moreover, the optical forces on the S-enantiomer work to confine the particle over the center of the dielectric channel while pushing the R-enantiomer away from the channel. Consequently, the potential wells for R- and S-enantiomers under CPL differ significantly (Figure 3f). In particular, the trapping potential is strong enough to trap S-enantiomers but is very shallow for R-enantiomers with thermal fluctuations sufficient to release them.

To experimentally quantify chiral optical forces, our group has developed chiral-optical force microscopy (CFM). Based on

atomic force microscopy (AFM), this method directly probes chiral-optical forces. ⁸⁵ In particular, CFM achieves both high force sensitivity in the pico-Newton range and high spatial resolution in the nanometer range. Our force measurement methodology is illustrated in Figure 4a. A chiral AFM tip is positioned at a specific height from a coaxial plasmonic aperture illuminated with CPL. By modulating the optical excitation at a certain frequency and monitoring the tip deflection at this frequency, we can extract the chiral optical forces exerted on the tip.

Using CFM, we quantified chiral optical forces from the coaxial aperture shown in Figure 4b; this particular plasmonic nanoaperture consists of a 60 nm dielectric (air) ring patterned in a 220 nm thick gold film. A concentric bull's-eye grating around the aperture further boosts the transmission efficiency. The resulting experimental transmission spectrum (Figure 4c) shows good agreement with simulations. Using a standard AFM silicon tip (Figure 4d inset), we measured the near-field optical forces exerted on the tip 50 nm from the aperture. As the laser

wavelength is swept, the spectral response of the optical forces measured by the tip precisely follows the spectral response of the aperture.

We next fabricated a chiral probe by focused ion beam milling a spiral pattern onto the AFM tip (Figure 4e); here, the chiral-optical response is determined by the spiral handedness, mimicking the interaction of a chiral specimen with the aperture near field. Figure 4f illustrates how CFM quantifies the contrast in total transverse optical forces upon left- and right-handed CPL illumination. The left-handed chiral tip is pulled toward the aperture when the handedness of the optical excitation matches that of the tip, while it is pushed away for optical excitation of opposite handedness. This force action decays with increasing tip-aperture distance, agreeing with full-field simulations of the resulting optical trapping potential (Figure 4g). This differential force is also evident for AFM tips with opposite chiralities, where a >15 pN differential between tips of opposite handedness is observed (Figure 4h).

This technique not only provides superior sensitivity to measure enantioselective optical forces, but can also create high spatial resolution maps of these forces. Figure 4i highlights such capability, showing a force map measured using a left-handed AFM tip scanned over the coaxial tweezers under both left- and right-handed CPL. Herein, the contrast between the two chiral forces is apparent and agrees well with simulations.

Beyond patterned chiral AFM tips, CFM can also measure the chiral-optical forces exerted on molecules, with future work aiming to detect dynamic conformation changes of chiral molecules functionalized to the tip. Therefore, coaxial plasmonic tweezers may not only enable on-chip chiral particle sorting, but also a new route for monitoring dynamic structural changes of few-to-single chiral macromolecules.

■ FUTURE PERSPECTIVES

In the pursuit of high sensitivity and high efficiency sensing and separation of chiral media, nanophotonics presents a myriad of platforms, from plasmonic to dielectric, chiral to achiral, and field-based to force-based. In this review, we described rational nanoantenna and metasurface design for chiral sensing and chiral photochemistry via strong magnetic resonances. We also highlighted the potential of plasmonic tweezers for enantioselective separation at the molecular level and the ability to quantify chiral optical forces with high sensitivity.

Improvements over state-of-the-art techniques to detect and achieve enantiopurity for pharmaceutical and agrochemical applications necessitate further enhancements in chiral-optical near-fields in the mid- to near-ultraviolet regimes, where most molecules of interest exhibit electronic resonances. While several materials, such as diamond, aluminum nitride, and titanium dioxide, are lossless into the UV, their lower refractive indices make confining light a challenge. Therefore, to approach the performance of current techniques, new methods to generate high magnetic field enhancements are necessary before enantioselective photoionization will be industrially relevant. One promising approach relies on accessing high-quality-factor modes through manipulation of symmetry. ^{69,86}

Additionally, theoretical approaches to model the electromagnetic interaction between chiral molecules and nanostructures often employ effective molecular medium models. Moving forward, studies would benefit from ab initio calculations that fully account for the excited-state electronic and vibrational modes of molecules and their interactions with those of classical or quantum nanophotonic systems. Further understanding of

chiral light—matter interactions with chemically modified surfaces and interfaces will provide new insight into mechanisms to enhance enantioselective absorption, ^{87–89} tailor chiral and spin selectivity in molecular electronic structure, ^{90,91} and tune induced circular dichroism in nanoparticles and assemblies. ^{92,93}

On a system level, the application of nanophotonic platforms must be optimized for high-throughput applications which maximize the enhancement between the engineered nanostructure near field and the analyte of interest. Examples of approaches to achieve large-scale chiral nanophotonic systems can include the efficient application of nano- and microfluidic channels or arrangements of multilayer metasurfaces. Further, the industrial-level development of chiral nanophotonic systems in dispersions or on flexible substrates can allow for an increase in interacting surface area between molecular matter and the engineered chiral evanescent fields. Effectively addressing these challenges will allow for technology transfer of promising research-scale chiral nanostructures toward highly effective alloptical chiral sensing and separation on an industrial scale.

AUTHOR INFORMATION

Corresponding Author

*E-mail: jdionne@stanford.edu.

ORCID ®

Michelle L. Solomon: 0000-0002-8123-7557 Amr A. E. Saleh: 0000-0001-7136-3683 Lisa V. Poulikakos: 0000-0002-1118-789X John M. Abendroth: 0000-0002-2369-4311 Jennifer A. Dionne: 0000-0001-5287-4357

Author Contributions

¹M.L.S. and A.A.E.S. contributed equally to this work. M.L.S. led authorship of the chiral sensing and photochemistry section. A.A.E.S. led authorship of the chiral optical forces section. L.V.P. and J.M.A. spearheaded the introduction and future perspectives sections and the literature survey, with help from L.F.T. J.A.D. advised on the scope and structure of the manuscript, with input from all authors, and supervised the work. All authors contributed to the editing of the manuscript.

Notes

The authors declare no competing financial interest.

Biographies

Michelle L. Solomon is a Ph.D. Candidate at Stanford University. Her research focuses on the use of dielectric nanophotonic structures to enhance chiral light—matter interactions for applications in sensing chiral molecules and separating enantiomers.

Amr A. E. Saleh received his Ph.D. in Electrical Engineering from Stanford University. He is currently a postdoctoral scholar at Stanford University; associate research director of the Microbial Detection and Identification (MDI) Center; and a lecturer in Engineering Physics at Cairo University. His research interests center on light—matter interactions at the nanoscale, particularly developing novel solutions for biological imaging and healthcare applications.

Lisa V. Poulikakos received her Ph.D. in Mechanical and Process Engineering from ETH Zurich and is now a postdoctoral researcher at Stanford University. Her research focuses on the development of theoretical and experimental nanophotonic platforms to controllably enhance the interaction between light and biological matter with a focus on chirality and tissue diagnostics.

John. M. Abendroth received his Ph.D. in Chemistry from the University of California, Los Angeles in 2018, and is currently a postdoctoral researcher at Stanford University. His research interests include enhancing chiral light—matter interactions for advanced spectroscopies, all-optical magnetic memory technologies, and chiral molecular spintronics.

Loza F. Tadesse is currently a Ph.D. candidate at Stanford University. Her research interest is in the applications of nanophotonic and plasmonic platforms for biomedical spectroscopy particularly Raman spectroscopy for bacterial diagnostics and antibiotic susceptibility testing.

Jennifer A. Dionne is an associate professor at Stanford University. She is also Director of Stanford's Photonics Research Center, the Photonics at Thermodynamic Limits EFRC, and the TomKat Center for Sustainable Energy. She received her Ph.D. in Applied Physics at Caltech and her postdoctoral training in Chemistry at Berkeley. Her research develops new materials to observe and control dynamic chemical and biological processes with nanometer scale resolution.

■ ACKNOWLEDGMENTS

The authors would like to thank Aitzol García-Etxarri, Chi-Sing Ho, and Yang Zhao, who were primary authors on several of the projects discussed in this Account. This paper, as well as the work that continues on the topic of chirality in the Dionne group, would not be possible without them. The authors would also like to thank Jack Hu and Mark Lawrence for their collaborations on these projects. The authors gratefully acknowledge the support of the Moore Inventors fellowship under Grant Number 6881, the National Science Foundation under Grant Number 1905209, and the Stanford "Catalyst for Collaborative Solutions" grant. M.L.S. acknowledges support from a National Defense Science and Engineering Graduate fellowship, L.V.P. acknowledges support from a Swiss National Science Foundation Early Postdoc Mobility fellowship under project number P2EZP2 181595, and L.F.T acknowledges support from Agilent, Stanford EDGE and Stanford DARE graduate fellowships.

REFERENCES

- (1) Barron, L. D. In *Chirality at the Nanoscale. Chirality at the Nanoscale*; Amabilino, D. B., Ed.; Wiley Online Library, 2009; pp 1–27.
- (2) Boriskina, S.; Zheludev, N. I. Singular and Chiral Nanoplasmonics; CRC Press, 2014.
- (3) Kahr, B. Polarization in France. Chirality 2018, 30, 351-368.
- (4) Rodger, A.; Nordén, B. Circular Dichroism and Linear Dichroism; Oxford University Press: Oxford, U.K., 1997.
- (5) Kemp, J. C. Piezo-Optical Birefringence Modulators: New Use for a Long-Known Effect. *J. Opt. Soc. Am.* **1969**, *59*, 950–954.
- (6) Richardson, F. S. Theory of Optical Activity in the Ligand-Field Transitions of Chiral Transition Metal Complexes. *Chem. Rev.* **1979**, 79, 17–36.
- (7) Smith, K. W.; Link, S.; Chang, W.-S. Optical Characterization of Chiral Plasmonic Nanostructures. *J. Photochem. Photobiol., C* **2017**, *32*, 40–57.
- (8) Tang, Y.; Cohen, A. E. Optical Chirality and Its Interaction with Matter. *Phys. Rev. Lett.* **2010**, *104*, 163901.
- (9) Poulikakos, L. V. Chiral Light—Matter Interactions in the Near and Far Field. Doctoral Thesis, ETH Zurich, 2018.
- (10) Lipkin, D. M. Existence of a New Conservation Law in Electromagnetic Theory. *J. Math. Phys.* **1964**, *5*, 696–700.
- (11) Papakostas, A.; Potts, A.; Bagnall, D. M.; Prosvirnin, S. L.; Coles, H. J.; Zheludev, N. I. Optical Manifestations of Planar Chirality. *Phys. Rev. Lett.* **2003**, *90*, 107404.

- (12) Gansel, J. K.; Thiel, M.; Rill, M. S.; Decker, M.; Bade, K.; Saile, V.; von Freymann, G.; Linden, S.; Wegener, M. Gold Helix Photonic Metamaterial as Broadband Circular Polarizer. *Science* **2009**, 325, 1513–1515.
- (13) Hendry, E.; Carpy, T.; Johnston, J.; Popland, M.; Mikhaylovskiy, R. V.; Lapthorn, A. J.; Kelly, S. M.; Barron, L. D.; Gadegaard, N.; Kadodwala, M. Ultrasensitive Detection and Characterization of Biomolecules Using Superchiral Fields. *Nat. Nanotechnol.* **2010**, *5*, 783–787
- (14) Hentschel, M.; Schäferling, M.; Weiss, T.; Liu, N.; Giessen, H. Three-Dimensional Chiral Plasmonic Oligomers. *Nano Lett.* **2012**, *12*, 2542–2547.
- (15) Zhao, Y.; Belkin, M. A.; Alù, A. Twisted Optical Metamaterials for Planarized Ultrathin Broadband Circular Polarizers. *Nat. Commun.* **2012**, *3*, 870.
- (16) Yin, X.; Schäferling, M.; Metzger, B.; Giessen, H. Interpreting Chiral Nanophotonic Spectra: The Plasmonic Born–Kuhn Model. *Nano Lett.* **2013**, *13*, 6238–6243.
- (17) Mark, A. G.; Gibbs, J. G.; Lee, T.-C.; Fischer, P. Hybrid Nanocolloids with Programmed Three-Dimensional Shape and Material Composition. *Nat. Mater.* **2013**, *12*, 802–807.
- (18) Schamel, D.; Pfeifer, M.; Gibbs, J. G.; Miksch, B.; Mark, A. G.; Fischer, P. Chiral Colloidal Molecules and Observation of the Propeller Effect. *J. Am. Chem. Soc.* **2013**, *135*, 12353–12359.
- (19) Schäferling, M.; Yin, X.; Engheta, N.; Giessen, H. Helical Plasmonic Nanostructures as Prototypical Chiral Near-Field Sources. *ACS Photonics* **2014**, *1*, 530–537.
- (20) McPeak, K. M.; van Engers, C. D.; Blome, M.; Park, J. H.; Burger, S.; Gosálvez, M. A.; Faridi, A.; Ries, Y. R.; Sahu, A.; Norris, D. J. Complex Chiral Colloids and Surfaces via High-Index Off-Cut Silicon. *Nano Lett.* **2014**, *14*, 2934–2940.
- (21) Yeom, J.; Yeom, B.; Chan, H.; Smith, K. W.; Dominguez-Medina, S.; Bahng, J. H.; Zhao, G.; Chang, W.-S.; Chang, S.-J.; Chuvilin, A.; Melnikau, D.; Rogach, A. L.; Zhang, P.; Link, S.; Krái, P.; Kotov, N. A. Chiral Templating of Self-Assembling Nanostructures by Circularly Polarized Light. *Nat. Mater.* 2015, *14*, 66–72.
- (22) Wang, L.-Y.; Smith, K. W.; Dominguez-Medina, S.; Moody, N.; Olson, J. M.; Zhang, H.; Chang, W.-S.; Kotov, N.; Link, S. Circular Differential Scattering of Single Chiral Self-Assembled Gold Nanorod Dimers. *ACS Photonics* **2015**, *2*, 1602–1610.
- (23) McPeak, K. M.; van Engers, C. D.; Bianchi, S.; Rossinelli, A.; Poulikakos, L. V.; Bernard, L.; Herrmann, S.; Kim, D. K.; Burger, S.; Blome, M.; et al. Ultraviolet Plasmonic Chirality from Colloidal Aluminum Nanoparticles Exhibiting Charge-Selective Protein Detection. *Adv. Mater.* **2015**, *27*, 6244–6250.
- (24) Tullius, R.; Karimullah, A. S.; Rodier, M.; Fitzpatrick, B.; Gadegaard, N.; Barron, L. D.; Rotello, V. M.; Cooke, G.; Lapthorn, A.; Kadodwala, M. Superchiral Spectroscopy: Detection of Protein Higher Order Hierarchical Structure with Chiral Plasmonic Nanostructures. *J. Am. Chem. Soc.* **2015**, *137*, 8380–8383.
- (25) Poulikakos, L. V.; Gutsche, P.; McPeak, K. M.; Burger, S.; Niegemann, J.; Hafner, C.; Norris, D. J. Optical Chirality Flux as a Useful Far-Field Probe of Chiral Near Fields. *ACS Photonics* **2016**, 3, 1619–1625.
- (26) Vázquez-Lozano, J. E.; Martínez, A. Optical Chirality in Dispersive and Lossy Media. *Phys. Rev. Lett.* **2018**, *121*, 043901.
- (27) Poulikakos, L. V.; Thureja, P.; Stollmann, A.; De Leo, E.; Norris, D. J. Chiral Light Design and Detection Inspired by Optical Antenna Theory. *Nano Lett.* **2018**, *18*, 4633–4640.
- (28) Schnoering, G.; Poulikakos, L. V.; Rosales-Cabara, Y.; Canaguier-Durand, A.; Norris, D. J.; Genet, C. Three-Dimensional Enantiomeric Recognition of Optically Trapped Single Chiral Nanoparticles. *Phys. Rev. Lett.* **2018**, *121*, 023902.
- (29) Kosters, D.; de Hoogh, A.; Zeijlemaker, H.; Acar, H.; Rotenberg, N.; Kuipers, L. Core—Shell Plasmonic Nanohelices. *ACS Photonics* **2017**, *4*, 1858—1863.
- (30) Hentschel, M.; Schäferling, M.; Duan, X.; Giessen, H.; Liu, N. Chiral Plasmonics. Sci. Adv. 2017, 3, e1602735.

(31) Karst, J.; Strohfeldt, N.; Schäferling, M.; Giessen, H.; Hentschel, M. Single Plasmonic Oligomer Chiral Spectroscopy. *Adv. Opt. Mater.* **2018**, *6*, 1800087.

- (32) Lee, H.-E.; Ahn, H.-Y.; Mun, J.; Lee, Y. Y.; Kim, M.; Cho, N. H.; Chang, K.; Kim, W. S.; Rho, J.; Nam, K. T. Amino-Acid- and Peptide-Directed Synthesis of Chiral Plasmonic Gold Nanoparticles. *Nature* **2018**, *556*, 360–365.
- (33) García-Guirado, J.; Svedendahl, M.; Puigdollers, J.; Quidant, R. Enantiomer-Selective Molecular Sensing Using Racemic Nanoplasmonic Arrays. *Nano Lett.* **2018**, *18*, 6279–6285.
- (34) Karst, J.; Cho, N. H.; Kim, H.; Lee, H.-E.; Nam, K. T.; Giessen, H.; Hentschel, M. Chiral Scatterometry on Chemically Synthesized Single Plasmonic Nanoparticles. *ACS Nano* **2019**, *13*, 8659–8668.
- (35) Valev, V. K.; Baumberg, J. J.; Sibilia, C.; Verbiest, T. Chirality and Chiroptical Effects in Plasmonic Nanostructures: Fundamentals, Recent Progress, and Outlook. *Adv. Mater.* **2013**, *25*, 2517–2534.
- (36) Ben-Moshe, A.; Maoz, B. M.; Govorov, A. O.; Markovich, G. Chirality and Chiroptical Effects in Inorganic Nanocrystal Systems with Plasmon and Exciton Resonances. *Chem. Soc. Rev.* **2013**, *42*, 7028–7041.
- (37) Kumar, J.; Eraña, H.; López-Martínez, E.; Claes, N.; Martín, V. F.; Solís, D. M.; Bals, S.; Cortajarena, A. L.; Castilla, J.; Liz-Marzán, L. M. Detection of Amyloid Fibrils in Parkinson's Disease Using Plasmonic Chirality. *Proc. Natl. Acad. Sci. U. S. A.* **2018**, *115*, 3225–3230.
- (38) Zhao, Y.; Xu, L.; Ma, W.; Wang, L.; Kuang, H.; Xu, C.; Kotov, N. A. Shell-Engineered Chiroplasmonic Assemblies of Nanoparticles for Zeptomolar DNA Detection. *Nano Lett.* **2014**, *14*, 3908–3913.
- (39) Kelly, C.; Tullius, R.; Lapthorn, A. J.; Gadegaard, N.; Cooke, G.; Barron, L. D.; Karimullah, A. S.; Rotello, V. M.; Kadodwala, M. Chiral Plasmonic Fields Probe Structural Order of Biointerfaces. *J. Am. Chem. Soc.* **2018**, *140*, 8509–8517.
- (40) Chen, W.; Bian, A.; Agarwal, A.; Liu, L.; Shen, H.; Wang, L.; Xu, C.; Kotov, N. A. Nanoparticle Superstructures Made by Polymerase Chain Reaction: Collective Interactions of Nanoparticles and a New Principle for Chiral Materials. *Nano Lett.* **2009**, *9*, 2153–2159.
- (41) Kuzyk, A.; Schreiber, R.; Fan, Z.; Pardatscher, G.; Roller, E.-M.; Högele, A.; Simmel, F. C.; Govorov, A. O.; Liedl, T. DNA-Based Self-Assembly of Chiral Plasmonic Nanostructures with Tailored Optical Response. *Nature* **2012**, *483*, 311–314.
- (42) Shen, X.; Song, C.; Wang, J.; Shi, D.; Wang, Z.; Liu, N.; Ding, B. Rolling up Gold Nanoparticle-Dressed DNA Origami into Three-Dimensional Plasmonic Chiral Nanostructures. *J. Am. Chem. Soc.* **2012**, *134*, 146–149.
- (43) Tang, Y.; Cohen, A. E. Enhanced Enantioselectivity in Excitation of Chiral Molecules by Superchiral Light. *Science* **2011**, 332, 333–336.
- (44) Tao, J.; Lin, G.-Q.; Liese, A. Biocatalysis for the Pharmaceutical Industry: Discovery, Development, and Manufacturing; John Wiley & Sons, 2009.
- (45) Schellman, J.; Jensen, H. P. Optical Spectroscopy of Oriented Molecules. *Chem. Rev.* **1987**, *87*, 1359–1399.
- (46) Seo, J. S.; Whang, D.; Lee, H.; Jun, S. I.; Oh, J.; Jeon, Y. J.; Kim, K. A Homochiral Metal—organic Porous Material for Enantioselective Separation and Catalysis. *Nature* **2000**, *404*, 982—986.
- (47) Ma, L.; Abney, C.; Lin, W. Enantioselective Catalysis with Homochiral Metal—organic Frameworks. *Chem. Soc. Rev.* **2009**, 38, 1248–1256.
- (48) Blaser, H. U.; Federsel, H.-J. Asymmetric Catalysis on Industrial Scale: Challenges, Approaches and Solutions; John Wiley & Sons, 2011.
- (49) Barrow, C. J.; Yasuda, A.; Kenny, P. T. M.; Zagorski, M. G. Solution Conformations and Aggregational Properties of Synthetic Amyloid β -Peptides of Alzheimer's Disease: Analysis of Circular Dichroism Spectra. *J. Mol. Biol.* **1992**, 225, 1075–1093.
- (50) Kumar, J.; Eraña, H.; López-Martínez, E.; Claes, N.; Martín, V. F.; Solís, D. M.; Bals, S.; Cortajarena, A. L.; Castilla, J.; Liz-Marzán, L. M. Detection of Amyloid Fibrils in Parkinson's Disease Using Plasmonic Chirality. *Proc. Natl. Acad. Sci. U. S. A.* **2018**, *115*, 3225–3230.

- (51) Neumann, O.; Zhang, D.; Tam, F.; Lal, S.; Wittung-Stafshede, P.; Halas, N. J. Direct Optical Detection of Aptamer Conformational Changes Induced by Target Molecules. *Anal. Chem.* **2009**, *81*, 10002—10006
- (52) Nakatsuka, N.; Yang, K.-A.; Abendroth, J. M.; Cheung, K. M.; Xu, X.; Yang, H.; Zhao, C.; Zhu, B.; Rim, Y. S.; Yang, Y.; et al. Aptamer—field-Effect Transistors Overcome Debye Length Limitations for Small-Molecule Sensing. *Science* **2018**, *362*, 319—324.
- (53) Kypr, J.; Kejnovska, I.; Renciuk, D.; Vorlickova, M. Circular Dichroism and Conformational Polymorphism of DNA. *Nucleic Acids Res.* **2009**, *37*, 1713–1725.
- (54) García-Etxarri, A.; Dionne, J. A. Surface-Enhanced Circular Dichroism Spectroscopy Mediated by Nonchiral Nanoantennas. *Phys. Rev. B: Condens. Matter Mater. Phys.* **2013**, *87*, 235409.
- (55) Gilroy, C.; Hashiyada, S.; Endo, K.; Karimullah, A. S.; Barron, L. D.; Okamoto, H.; Togawa, Y.; Kadodwala, M. Roles of Superchirality and Interference in Chiral Plasmonic Biodetection. *J. Phys. Chem. C* **2019**, *123*, 15195–15203.
- (56) Ho, C.-S.; Garcia-Etxarri, A.; Zhao, Y.; Dionne, J. Enhancing Enantioselective Absorption Using Dielectric Nanospheres. *ACS Photonics* **2017**, *4*, 197–203.
- (57) Solomon, M. L.; Hu, J.; Lawrence, M.; García-Etxarri, A.; Dionne, J. A. Enantiospecific Optical Enhancement of Chiral Sensing and Separation with Dielectric Metasurfaces. *ACS Photonics* **2019**, *6*, 43–49.
- (58) Kerker, M.; Wang, D.-S.; Giles, C. L. Electromagnetic Scattering by Magnetic Spheres. *J. Opt. Soc. Am.* **1983**, *73*, *765*–*767*.
- (59) Staude, I.; Miroshnichenko, A. E.; Decker, M.; Fofang, N. T.; Liu, S.; Gonzales, E.; Dominguez, J.; Luk, T. S.; Neshev, D. N.; Brener, I.; et al. Tailoring Directional Scattering through Magnetic and Electric Resonances in Subwavelength Silicon Nanodisks. *ACS Nano* **2013**, *7*, 7824–7832.
- (60) Mohammadi, E.; Tavakoli, A.; Dehkhoda, P.; Jahani, Y.; Tsakmakidis, K. L.; Tittl, A.; Altug, H. Accessible Superchiral Near-Fields Driven by Tailored Electric and Magnetic Resonances in All-Dielectric Nanostructures. *ACS Photonics* **2019**, *6*, 1939–1946.
- (61) Inoue, Y. Asymmetric Photochemical Reactions in Solution. *Chem. Rev.* **1992**, 92, 741–770.
- (62) Balavoine, G.; Moradpour, A.; Kagan, H. B. Preparation of Chiral Compounds with High Optical Purity by Irradiation with Circularly Polarized Light, a Model Reaction for the Prebiotic Generation of Optical Activity. *J. Am. Chem. Soc.* **1974**, *96*, 5152–5158.
- (63) Flores, J. J.; Bonner, W. A.; Massey, G. A. Asymmetric Photolysis of (RS)-Leucine with Circularly Polarized Ultraviolet Light. *J. Am. Chem. Soc.* 1977, 99, 3622–3625.
- (64) Wang, L.; Yin, L.; Zhang, W.; Zhu, X.; Fujiki, M. Circularly Polarized Light with Sense and Wavelengths To Regulate Azobenzene Supramolecular Chirality in Optofluidic Medium. *J. Am. Chem. Soc.* **2017**, *139*, 13218–13226.
- (65) Huck, N. P. M.; Jager, W. F.; de Lange, B.; Feringa, B. L. Dynamic Control and Amplification of Molecular Chirality by Circular Polarized Light. *Science* **1996**, *273*, 1686–1688.
- (66) Kuhn, W.; Braun, E. Photochemische Erzeugung Optisch Aktiver Stoffe. *Naturwissenschaften* **1929**, *17*, 227–228.
- (67) Feringa, B.; Wynberg, H. Biomimetic Asymmetric Oxidative Coupling of Phenols. *Bioorg. Chem.* **1978**, *7*, 397–408.
- (68) Kuhn, W. Optical Rotatory Power. Annu. Rev. Phys. Chem. 1958, 9, 417–438.
- (69) Hu, J.; Lawrence, M.; Dionne, J. A. High Quality Factor Dielectric Metasurfaces for Ultraviolet Circular Dichroism Spectroscopy. *ACS Photonics* **2019**, DOI: 10.1021/acsphotonics.9b01352.
- (70) Banerjee-Ghosh, K.; Ben Dor, O.; Tassinari, F.; Capua, E.; Yochelis, S.; Capua, A.; Yang, S.-H.; Parkin, S. S. P.; Sarkar, S.; Kronik, L.; et al. Separation of Enantiomers by Their Enantiospecific Interaction with Achiral Magnetic Substrates. *Science* **2018**, *360*, 1331–1334.
- (71) Tassinari, F.; Steidel, J.; Paltiel, S.; Fontanesi, C.; Lahav, M.; Paltiel, Y.; Naaman, R. Enantioseparation by Crystallization Using Magnetic Substrates. *Chem. Sci.* **2019**, *10*, 5246–5250.

(72) Ashkin, A.; Dziedzic, J. M.; Bjorkholm, J. E.; Chu, S. Observation of a Single-Beam Gradient Force Optical Trap for Dielectric Particles. *Opt. Lett.* **1986**, *11*, 288.

- (73) Ashkin, A.; Dziedzic, J. M.; Yamane, T. Optical Trapping and Manipulation of Single Cells Using Infrared Laser Beams. *Nature* **1987**, 330, 769–771.
- (74) Fazal, F. M.; Block, S. M. Optical Tweezers Study Life under Tension. *Nat. Photonics* **2011**, *5*, 318–321.
- (75) Fazal, F. M.; Meng, C. A.; Murakami, K.; Kornberg, R. D.; Block, S. M. Real-Time Observation of the Initiation of RNA Polymerase II Transcription. *Nature* **2015**, *525*, *274*–*277*.
- (76) Tkachenko, G.; Brasselet, E. Optofluidic Sorting of Material Chirality by Chiral Light. *Nat. Commun.* **2014**, *5*, 3577.
- (77) Canaguier-Durand, A.; Hutchison, J. A.; Genet, C.; Ebbesen, T. W. Mechanical Separation of Chiral Dipoles by Chiral Light. *New J. Phys.* **2013**, *15*, 123037.
- (78) Canaguier-Durand, A.; Genet, C. Chiral Route to Pulling Optical Forces and Left-Handed Optical Torques. *Phys. Rev. A: At., Mol., Opt. Phys.* **2015**, 92, 043823.
- (79) Canaguier-Durand, A.; Genet, C. Plasmonic Lateral Forces on Chiral Spheres. J. Opt. **2016**, *18*, 015007.
- (80) Wang, S. B.; Chan, C. T. Lateral Optical Force on Chiral Particles near a Surface. *Nat. Commun.* **2014**, *5*, 3307.
- (81) Zhao, Y.; Saleh, A. A. E.; Dionne, J. A. Enantioselective Optical Trapping of Chiral Nanoparticles with Plasmonic Tweezers. *ACS Photonics* **2016**, *3*, 304–309.
- (82) Sihvola, A. H.; Viitanen, A. J.; Lindell, I. V.; Tretyakov, S. A. Electromagnetic Waves in Chiral and Bi-Isotropic Media; Artech House, 1994.
- (83) Saleh, A. A. E.; Dionne, J. A. Toward Efficient Optical Trapping of Sub-10-Nm Particles with Coaxial Plasmonic Apertures. *Nano Lett.* **2012**, *12*, 5581–5586.
- (84) Yoo, D.; Gurunatha, K. L.; Choi, H.-K.; Mohr, D. A.; Ertsgaard, C. T.; Gordon, R.; Oh, S.-H. Low-Power Optical Trapping of Nanoparticles and Proteins with Resonant Coaxial Nanoaperture Using 10 Nm Gap. *Nano Lett.* **2018**, *18*, 3637–3642.
- (85) Zhao, Y.; Saleh, A. A. E.; van de Haar, M. A.; Baum, B.; Briggs, J. A.; Lay, A.; Reyes-Becerra, O. A.; Dionne, J. A. Nanoscopic Control and Quantification of Enantioselective Optical Forces. *Nat. Nanotechnol.* **2017**, *12*, 1055–1059.
- (86) Lawrence, M.; Dionne, J. A. Nanoscale Nonreciprocity via Photon-Spin-Polarized Stimulated Raman Scattering. *Nat. Commun.* **2019**, *10*, 3297.
- (87) Nesterov, M. L.; Yin, X.; Schäferling, M.; Giessen, H.; Weiss, T. The Role of Plasmon-Generated Near Fields for Enhanced Circular Dichroism Spectroscopy. *ACS Photonics* **2016**, *3*, 578–583.
- (88) Lee, S.; Yoo, S.; Park, Q.-H. Microscopic Origin of Surface-Enhanced Circular Dichroism. *ACS Photonics* **2017**, *4*, 2047–2052.
- (89) Kneer, L. M.; Roller, E.-M.; Besteiro, L. V.; Schreiber, R.; Govorov, A. O.; Liedl, T. Circular Dichroism of Chiral Molecules in DNA-Assembled Plasmonic Hotspots. *ACS Nano* **2018**, *12*, 9110–9115.
- (90) Abendroth, J. M.; Stemer, D. M.; Bloom, B. P.; Roy, P.; Naaman, R.; Waldeck, D. H.; Weiss, P. S.; Mondal, P. C. Spin Selectivity in Photoinduced Charge-Transfer Mediated by Chiral Molecules. *ACS Nano* **2019**, *13*, 4928–4946.
- (91) Bloom, B. P.; Graff, B. M.; Ghosh, S.; Beratan, D. N.; Waldeck, D. H. Chirality Control of Electron Transfer in Quantum Dot Assemblies. *J. Am. Chem. Soc.* **2017**, *139*, 9038–9043.
- (92) Moloney, M. P.; Govan, J.; Loudon, A.; Mukhina, M.; Gun'ko, Y. K. Preparation of Chiral Quantum Dots. *Nat. Protoc.* **2015**, *10*, 558–573.
- (93) Slocik, J. M.; Govorov, A. O.; Naik, R. R. Plasmonic Circular Dichroism of Peptide-Functionalized Gold Nanoparticles. *Nano Lett.* **2011**, *11*, 701–705.